563578

AIAA 2001-0078

Experimental Investigation of 'Transonic Resonance' with Convergent-Divergent Nozzles

K. B. M. Q. Zaman, M. D. Dahl
and T. J. Bencic

NASA Glenn Research Center
Cleveland, OH 44135

39th AIAA Aerospace Sciences Meeting & Exhibit
8-11 January 2001 / Reno, NV

Experimental Investigation of 'Transonic Resonance' with Convergent-Divergent Nozzles

by

K. B. M. Q. Zaman*, M. D. Dahl† and T. J. Bencic‡
NASA Glenn Research Center
Cleveland, OH 44135

Abstract

Convergent-divergent nozzles, when run at pressure ratios lower than the design value, often undergo a flow resonance accompanied by the emission of acoustic tones. The phenomenon, different in characteristics from conventional 'screech' tones, has been studied experimentally. Unlike screech, the frequency increases with increasing supply pressure. There is a 'staging' behavior; 'odd harmonic' stages resonate at lower pressures while the fundamental occurs in a range of higher pressures corresponding to a fully expanded Mach number (M_j) around unity. The frequency (f_N) variation with M_j depends on the half angle-of-divergence (θ) of the nozzle. At smaller θ, the slope of f_N versus M_j curve becomes steeper. The resonance involves standing waves and is driven by unsteady shock / boundary layer interaction. The distance between the foot of the shock and the nozzle exit imposes the length-scale (L'). The fundamental corresponds to a quarter-wave resonance, the next stage at a lower supply pressure corresponds to a three-quarter-wave resonance, and so on. The principal trends in the frequency variation are explained simply from the characteristic variation of the length-scale L'. Based on the data, correlation equations are provided for the prediction of f_N. A striking feature is that tripping of the boundary layer near the nozzle's throat tends to suppress the resonance. In a practical nozzle a tendency for the occurrence of the phenomenon is thought to be a source of 'internal noise'; thus, there is a potential for noise benefit simply by appropriate boundary layer tripping near the nozzle's throat.

1. Introduction

Flow through a nozzle, especially one involving area change and sudden expansion, often encounters aeroacoustic resonance. Nozzles with sudden expansion, e.g., 'whistler nozzles', have been studied in this regard by Hill & Greene[1] for incompressible flows and by Hussain & Hasan[2] at higher subsonic Mach numbers. Similar flows involving choked and supersonic conditions have been addressed by Witczak[3] and by Krothapalli & Hsia.[4] The resonance in many cases could be traced to a coupling between the organ pipe, or duct acoustic, modes and the instability of the shear layer separated from the sudden expansion. With supersonic flows, screech tones from imperfectly expanded jets (Refs. 5-7), which themselves involve a not-so-well-understood feedback loop, could come into play and interact with the duct acoustic modes to set up a more complex resonance.[4]

The present study concerns convergent-divergent nozzles involving a smooth convergence to the throat and then a smooth divergence up to the exit without any sudden area change. Resonance and tones are also encountered with such a nozzle. As the pressure driving the flow is gradually increased to reach an operating condition, or when the flow is gradually brought to a halt from the operating condition, tones of various frequencies may be heard. Most well known are the

* Nozzle Branch, Associate fellow, AIAA
† Acoustics Branch, Member, AIAA
‡ Optical Instrumentation Technology Branch, Member, AIAA

screech tones that take place at relatively large pressures involving off-design, overexpanded or underexpanded, conditions. Tones can also occur at very low pressures with entirely subsonic flow often due to flow-induced acoustic resonance of various components of the jet facility. In the present study the focus is on an intermediate range of pressures, when a shock exists within the diverging section of the nozzle. In this pressure range, that could be operative under certain off-design run condition, the flow often locks on to a resonance accompanied by very loud tones.

Such tones have been observed with C-D nozzles by others "as a precursor to screech",[8] as well as with subsonic diffusers by the authors.[9] About two decades ago, a series of experiments was conducted with a two-dimensional diffuser run at 'transonic' conditions.[10-13] A similar self-excited flow oscillation was observed; this, and some other relevant work, will be discussed in the text. However, a literature search on nozzle aerodynamics and jet noise yielded virtually no other documentation of the phenomenon. Even though it is just as intense as screech tones, to the authors' knowledge, there has not been any report or recognition of it in the vast literature dealing with screech. Our first investigation was conducted about two years ago.[14] Those results, distinguishing the phenomenon from conventional screech tones, will be summarized in §3.1. However, full details remained far from clear and the study was continued. This was justified since apart from academic curiosity, the phenomenon had significant practical relevance. The reader may appreciate this relevance from a cursory review of Figs. 1 and 2.

The frequency variations of the resonance for a variety of nozzles are shown in Fig. 1. For these data, the jet from a given nozzle exhausted in to the ambient of the test chamber. The tone frequency was measured by spectral analysis of the signal from a suitably placed microphone. The figure includes data from nozzles as small as ¼ inch in diameter to as large as 3½ inches in diameter (table 1; notations are explained in §2). There is also a set of data from a rectangular nozzle, and another set from a circular, coannular nozzle having a convergent-divergent outer annulus. These data make it amply clear that the phenomenon is quite common, at least in laboratory environment, and must be understood when considering mixing and noise of the ensuing jet. (The dashed lines passing through the data point on the

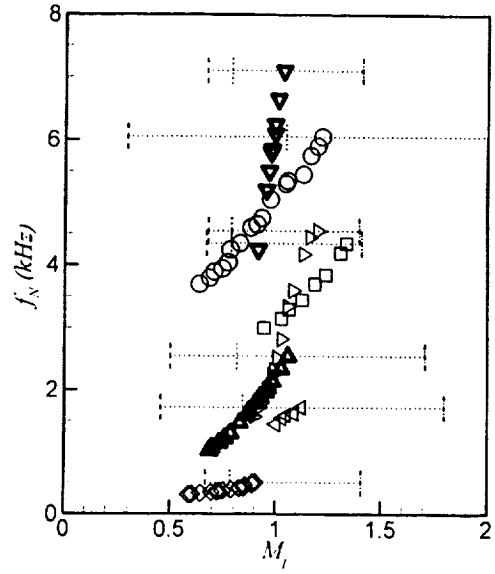

Fig. 1 Tone frequency variation with M_j for several convergent-divergent nozzles listed in table 1: ○, **nozzle #1;** □, **#2;** ◁, **#3;** ▷, **#4;** ◊, **#5;** ▽, **#6;** △, **#7.**

Table 1 Dimensions of nozzles of Fig. 1 and Ref. 14.

Nozzle	Shape	D_j (in)	D_e (in)	L (in)	θ (deg.)
1	Circular	0.25	0.36	0.375	8.34
2	Circular	0.25	0.36	0.75	4.20
3	Circular	0.836	1.0	1.36	3.45
4	Circular	0.95	1.0	0.866	1.65
5	Circular	2.565	3.5	4.20	6.35
6	Rect-angular	1.056 (2.8 x 0.313)	1.117 (2.8 x 0.35)	0.325	1.85*
7	Co-axial (C-D outer annulus)	1.197	1.391 (2.075, 1.54)	1.00	1.46*
8	Circular	0.25	0.302	0.512	2.91
9	Circular	0.25	0.261	0.236	1.34

* see definition in §4.2

right in each set represent flow regimes based on one-dimensional nozzle flow analysis, discussed in §3.1).

A striking feature of the phenomenon is that it requires a clean and smooth interior of the nozzle. Figure 2 shows noise spectra for the coannular nozzle.[15] The resonance takes place in the outer annulus that is convergent-divergent. The solid curve represents normal run condition with a smooth interior; the sharp

spike at 1.63 kHz is the resonant frequency. The dashed curve represents the same operating condition except that the boundary layer in the outer annulus is tripped just upstream of the throat. The trip practically suppresses the tone; however, an inspection reveals that there is still some energy at the resonant frequency. In fact, it took several trials with the boundary layer trip to achieve the best suppression as shown. This implies that in a practical nozzle, often with non-ideal geometry and conditions, the subject resonance may not be a problem outright but its mechanism may still be in play. The resultant contribution to jet noise may not be negligible; the residual peak in the dashed curve has contributed more than one-half of a dB to the overall sound pressure level. Indeed, the phenomenon may be a source of 'internal noise' in a nozzle system. The importance of identifying such a source may be appreciated from the viewpoint of jet noise reduction efforts. In the development of a nozzle for modern aircraft, often one has to go to great lengths, with liners on ejector interiors, for example, to absorb internal noise.

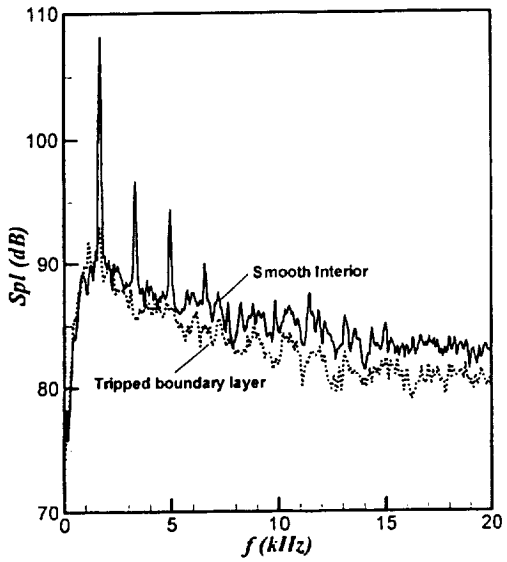

Fig. 2 Sound pressure level spectra for nozzle 7T1 (nozzle #7 of table 1; co-annular case). Outer jet Mach number, M_{jo} = 0.86, inner jet Mach number, M_{ji} = 1.02. Boundary layer trip applied to interior of outer nozzle.

Apart from the relevance discussed with the help of Figs. 1 and 2, the phenomenon may also be pertinent to unsteady transonic flows in various components of a supersonic propulsion system. It involves shock / boundary layer interaction followed by adverse pressure gradients that are also ingredients for "...dynamic distortion in inlets, pressure oscillations in ramjets, buffeting in external flows, and possibly certain types of compressor stalls" (Ref. 12). It is possible that the unsteadiness reported for diffusers,[12] nozzles,[16,17] as well as wing sections,[18,19] are of similar origin. Certain rocket engine instabilities (see, e.g., Ref. 20) might be coupled to similar unsteady flows in the exhaust nozzle. As it will become clear, the flow unsteadiness is internal to the nozzle and, thus, the aerodynamic loads are large. Therefore, this may pose a threat for structural fatigue of nozzles more serious than that posed by conventional screech tones (see Ref. 7 for a discussion of the latter). A continued study of the phenomenon was therefore considered well justified.

In the following, results from primarily single, round, convergent-divergent nozzles are considered. The main aim has been to advance the understanding of the phenomenon while seeking engineering correlations for prediction of its frequency and methods for its suppression. The experimental procedures are given in §2. In §3, first a brief summary of earlier results (Ref. 14) is given. Recent results on further characteristics of the phenomenon are then documented. Frequency scaling is addressed with results from sets of nozzles having dimensions varied systematically. The steady flow pattern on the nozzle's internal wall is examined via a temperature-sensitive-paint technique. Unsteady flow measurements, carried out inside the nozzle using a miniature pressure probe, are discussed in an effort to shed light on to the flow mechanism. Finally, in §4, results from certain past works are compared before providing a summary of the investigation.

2. Experimental Procedure

The data were obtained in three different open jet facilities of different size. In all facilities, compressed air passed through a cylindrical plenum chamber fitted with flow conditioning units and then through the nozzle to discharge into the quiescent ambient. The diameters of the plenum chamber in the three facilities were 30 in, 10 in and 5 in; some further description can be found in Ref. 21. All experiments involved 'cold' flows, i.e., the jet was unheated and the total temperature was approximately the same throughout and equaled that in the ambient.

In table 1, nozzles 3 through 7 were made of aluminum and the rest were made of clear plastic. The aluminum nozzles had a 'normally' machined surface finish. The surface 'roughness height deviation' in most cases was estimated to be about 64 microinches. Some of the plastic nozzles were polished, with the application of 'scratch removal compound', to enable clear visualization of the internal flow. The roughness height deviation in those cases was estimated to be within 16 micorinches. Some of the nozzles (#3,4,8 and 9) were designed and contoured following the method of characteristics. In other cases, less rigorous criteria were followed, however, all junctions were faired and smooth transition was ensured. In the following, the throat-to-exit area ratio is used to estimate the state of the flow based on one-dimensional analysis. As it will become apparent, the throat-to-exit axial length, L as well as the half-angle of divergence ($\theta = \tan^{-1}((D_e - D_t)/2L)$) turn out to be important parameters determining the frequency characteristics. Here, D_e and D_t are the exit and throat diameters of the nozzle, respectively. In table 1, D_e and D_t for nozzles 6 and 7 are equivalent diameters based on the exit and throat areas.

In order to address the frequency scaling, a set of plastic nozzles was fabricated. All had identical convergent sections and a nominal throat diameter, $D_t = 0.3$ in. The divergent section in these cases was a straight cone starting at 0.050 in from the throat; the transition was faired smoothly. While keeping D_t a constant, L and D_e were varied. The dimensions of the divergent section of these nozzles are given in table 2. (In the following a given nozzle will be identified by its number followed by the table number; e.g., '1T2' will denote nozzle 1 of table 2). Some of the nozzles of table 2 had to be resurfaced and repolished in order for the resonance to take place prominently. This explains the somewhat larger throat diameter for some of the cases. In addition to the nozzles listed in table 2, another set of experiments was conducted starting with nozzle 2T2 and then trimming it off in steps to provide lengths of 1.3, 1.1, 0.9, 0.75, 0.6 and 0.495 inches. Thus, for this set both L and D_e varied but the half-angle (θ) remained approximately a constant. (The value of θ actually decreased somewhat for small L due to the fairing near the throat.) Various combinations of these nozzles permitted the examination of the parametric dependence of the resonant frequency.

The frequency data were obtained from spectral analysis of the sound measured with a microphone. The bandwidth was chosen such that the accuracy of the measured tone frequency was within 1%. The 'jet Mach number', $M_j = (((p_0/p_a)^{(\gamma-1)/\gamma} - 1)\frac{2}{\gamma-1})^{1/2}$, is used as the independent variable. Here, p_0 and p_a are plenum pressure and ambient pressure, respectively. The uncertainty in the measurement of M_j is also well within 1%. Some other nozzle configurations and experimental procedures will be discussed along with the results.

Table 2 Dimensions of the nozzles for frequency-scaling study

Nozzle	D_t (in)	D_e (in)	L (in)	θ (deg.)
1	0.307	0.400	3.00	0.89
2	0.304	0.400	1.50	1.83
3	0.300	0.400	0.75	3.81
4	0.304	0.400	0.48	5.71
5	0.300	0.400	0.375	7.59
6	0.300	0.320	0.75	0.76
7	0.300	0.500	0.75	7.59

3. Results

3.1 Distinction from screech tones: Figures 3-6 summarizes earlier results discussed in Ref. 14. These illustrate salient features of the resonance and its difference from conventional screech tones. Variations of frequency and amplitude of the tone for nozzle 3T2 are shown in Fig. 3. The band of frequency data on the right represents screech tone. This is recognized as such from the characteristic frequency variation (decreasing with increasing M_j) and also from a comparison of the Strouhal number with data from the literature. The 'transonic resonance' takes place in two stages, as represented by the two bands of frequency data on the left. These are marked (1) and (2) in the figure. A difference in the trend is immediately apparent. Unlike screech, the frequency in both stages increases with increasing M_j. *Another important and pertinent distinction is that the 'transonic tones' occur only with C-D nozzles and not with a convergent nozzle.* In contrast, screech tones, in fact, have been studied mostly with choked flows from convergent nozzles. The results of Fig. 3 demonstrate another aspect. The tone amplitudes are shown on the top (ordinate on right). It can be seen that the transonic tones are loud, often louder than the screech tones.

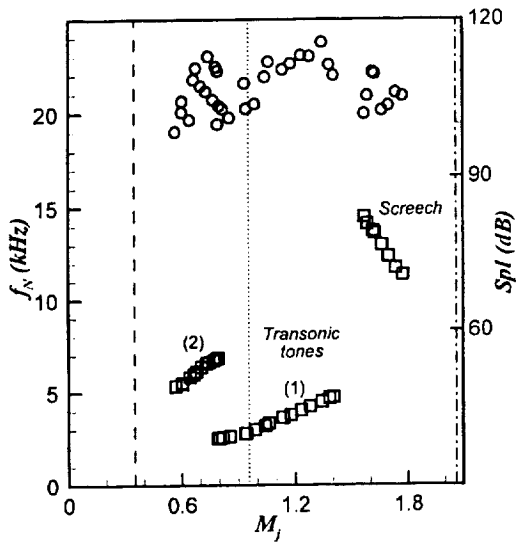

Fig. 3 Variation of frequency (□) and amplitude (O) of tones with M_j for nozzle 3T2 ($D_t = 0.3, D_e = 0.4, L = 0.75$).

In Fig. 3, the vertical lines demarcate flow regimes deduced from one-dimensional nozzle flow analysis, based on exit-to-throat area ratio. From the left, the first (dashed line) represents condition when the flow is just choked, the second (dotted line) when a 'normal shock' is expected at the nozzle exit, and the third (chain-dashed line) when the flow is perfectly expanded. Thus, to the left of the dashed line the flow is subsonic, between the dashed and dotted lines a shock is expected in the diverging section, between the dotted and the chain-dashed lines the flow is overexpanded, and to the right of the chain-dashed line the flow is underexpanded. (These regimes were demarcated for each dataset in Fig. 1). It can be seen that the resonance takes place when a shock exists within the divergent section or when the flow is apparently in the early stage of overexpansion. Many other nozzles also exhibited two stages of the resonance. Stage (1) resonance on the right was typically dominant and involved the loudest tones. Data for only this stage was shown in Fig. 1. The staging behavior is further addressed in the following.

Frequency data for nozzle 8T1 are shown in Fig. 4. The band of data on the right again represents screech. Here, three stages are observed for the transonic tones. There are overlaps between stages where peaks at both frequencies occur in the time-averaged spectrum; the frequencies are not exact harmonics of each other. The square and circular symbols represent data taken in two different jet facilities with the same nozzle. It is clear that the transonic tones are independent of the facility and thus, characteristic of the nozzle. Occasionally, tones would occur when the flow is entirely subsonic; one such data point is shown on the left of the dashed vertical line. Some of these are not reproducible from one facility to another. These appear to be related to either facility resonance or other unknown sources and are ignored for the rest of the paper.

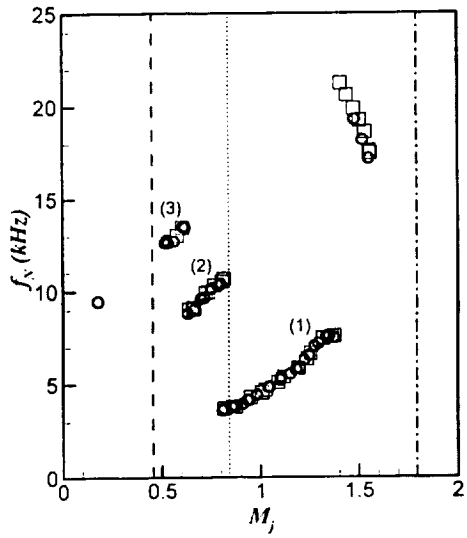

Fig. 4 Tone frequency variation for nozzle 8T1(D_t = 0.25, D_e = 0.302, L = 0.512): □, data from a small jet facility; O, data from the large jet facility.

Figure 5 shows sound pressure level spectra for nozzle 9T1. Data for three values of M_j are shown, there being a pair of traces at each M_j. The dotted lines represent spectra obtained with two tabs installed at the nozzle exit.[22] It is apparent that while screech is eliminated by the tabs (at the highest M_j), the tones at the two lower M_j are affected only little. The small effect (somewhat lower frequency and amplitude) could be due to blockage by the tabs. It should be noted that a relatively large tab (e.g., the end of a small flat-headed screw-driver inserted sufficiently into the flow) would eliminate the tone completely. But this apparently occurs due to a shift of the choke location to the exit, when the nozzle acts like a convergent one. Results of Fig. 5 suggest that the origin of the tone under consideration is internal to the nozzle, and this is confirmed by the boundary layer trip effect discussed next.

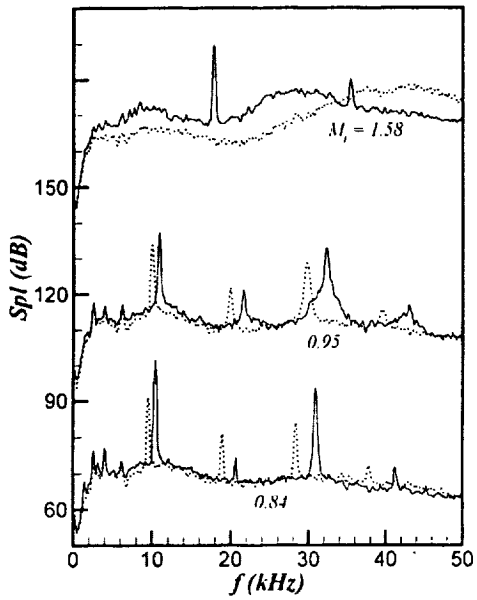

Fig. 5 Sound pressure level spectra for nozzle 9T1 (D_t = 0.25, D_e = 0.261, L = 0.236). Three pairs of spectra, staggered by 40 dB, are for indicated values of M_j (ordinate pertains to the pair at the bottom). Solid curves, normal operation; dotted curves, with two tabs at exit.

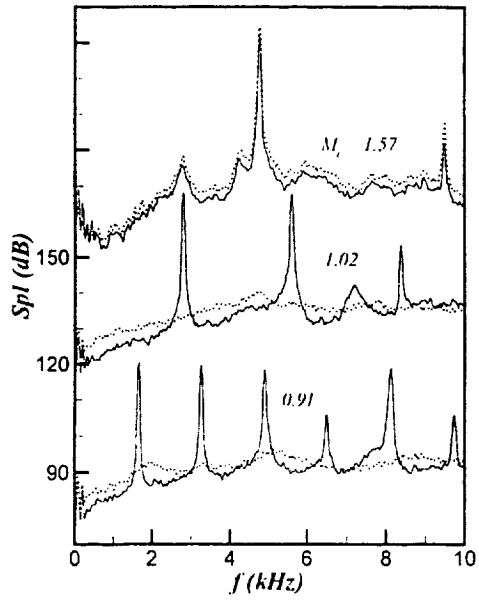

Fig. 6 Sound pressure level spectra as in Fig. 5 for nozzle 4T1 (D_t = 0.95, D_e = 1.0, L = 0.866): solid curves, smooth interior of nozzle; dotted curves, tripped boundary layer.

Sound pressure level spectra, with and without boundary layer trip applied just prior to the throat, are shown in Fig. 6 for nozzle 4T1. Data for three values of M_j are presented similarly as in Fig. 5. The trip comprised of four ½ in wide pieces of adhesive tape (approximately 0.003 in thick) placed close to but sufficiently upstream of the throat so that there was no change in the minimum (throat) area. These were spaced equally on the periphery. As it can be seen, at the highest M_j, there was no effect on screech. This is expected because screech occurs due to a feedback loop that is external to the nozzle. However, boundary layer trip essentially eliminated the transonic tones at the lower values of M_j. Similar result was shown for nozzle 3T1 (Ref. 14), as well as for nozzle 7T1 in Fig. 2.

Further investigation of the boundary layer trip effect: The effect of boundary layer trip location was explored further with nozzle 3T1. Four epoxy beads, each approximately 0.08 in across and 0.005 in high, were applied at a given axial location spaced equally on the internal periphery of the nozzle. The tone amplitudes were examined at two operating conditions: M_j = 1.0 (f_N = 1.55 kHz) and M_j = 0.89 (f_N = 3.6 kHz). With the beads located 0.3 in upstream of the throat the amplitudes reduced by about 80%; however, small but clear peaks remained in the spectrum. Practically a complete suppression was achieved when the beads were located about 0.3 in downstream of the throat. However, with the latter location the effect was inconsistent at other pressures (i.e., the tone reappeared). On the other hand, when the beads were moved farther downstream the effectiveness diminished rapidly. It was apparent that the trip needed to be placed upstream of the location of the shock (and shock-induced boundary layer separation). This will become clearer later.

It should be emphasized that the trip affected the amplitude but seldom the frequency of the tone. The amplitude was indeed sensitive to the surface texture near the throat. For example, when the trips were removed, inadvertent smudges left behind would affect the tone and the amplitude would not reproduce exactly.

3.2 Frequency scaling: Parametric dependence of the frequency of the transonic tone is now addressed. At first data for stage 1 is considered only. Figure 7 shows data for varying length of the divergent section, L, while

D_t and D_e are held approximately constant (nozzles 1 through 5 of table 2). It can be seen that the frequency, at a given M_j, increases with decreasing L. Figure 8 shows similar data for varying D_e, while D_t and L are held constants (note that the half-angle θ also varies with D_e). The slope of the frequency variation curve can

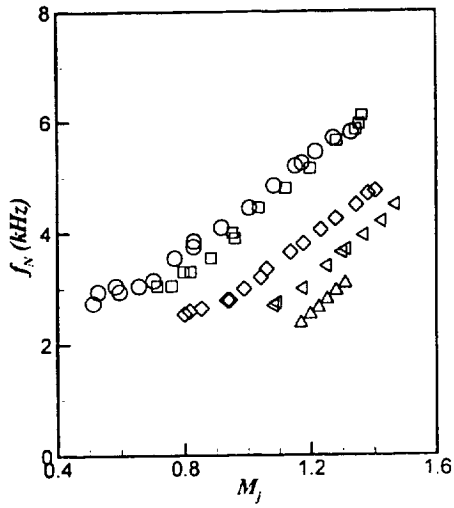

Fig. 7 Frequency variation (stage 1) for nozzles of constant throat and exit diameters ($D_t \approx 0.3$ in and $D_e = 0.4$) but different throat-to-exit length L (table 2). Δ, 3.0 (#1); ◁, 1.5 (#2); ◊, 0.75 (#3); □, 0.48 (#4), O, 0.375 (#5).

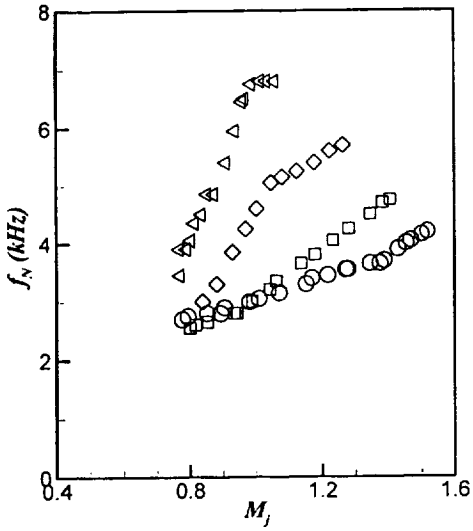

Fig. 8 Frequency variation (stage 1) for nozzles of constant D_t and L but different D_e (table 2). O, 0.5 in (#7); □, 0.4 in (#3); ◊, 0.35 in (#2, trimmed); ◁, 0.32 in (#6).

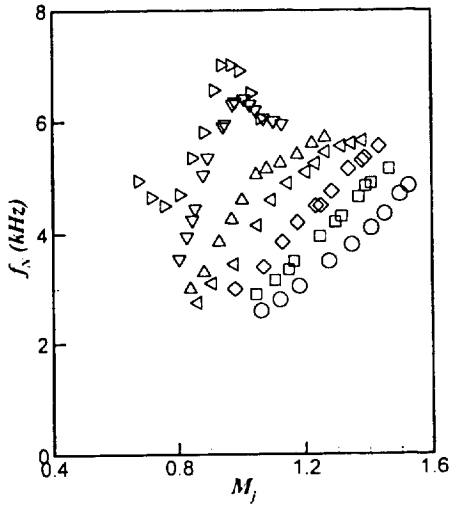

Fig. 9 Frequency variation (stage 1) for nozzle 2T2 (D_t = 0.304) trimmed to different length: O, L=1.5; □, 1.3; ◊, 1.1; ◁, 0.9; Δ, 0.75; ▽, 0.6; ▷, 0.495.

be seen to steepen with decreasing θ. Furthermore, for small values of θ, a departure from the approximately linear trend is observed especially on the far right. Finally, data for the 'trimmed' cases with nozzle 2T2 are shown in Fig. 9. A trend similar to that observed in Fig. 7 may be noted. That is, frequency increases with decreasing L. There is also a clear departure from linear variation at small values of θ– the frequency actually decreases with increasing M_j.

The scaling of the data of Figs. 7-9 is now examined. Data of Fig. 9 are replotted in nondimensionalized ($f_N L/a_0$) form in Fig. 10(a); here, a_0 is the speed of sound in the ambient. The data have collapsed quite well (except for deviations on far right of each curve). Thus, the frequency, on a first approximation, simply scales as the length of the diverging section. The same, however, is not true for the data of Fig. 7, shown in nondimensional form in Fig. 10(b).

In Fig. 10(b), the curves are close to one another for smaller values of L; however, there is progressive departure with increasing L for the given D_t and D_e. This observation posed a stumbling block in the understanding of the frequency scaling at the time the abstract of this paper was submitted. It was not clear if the much higher nondimensional values for large L were due to a 'staging' behavior or some other factor.

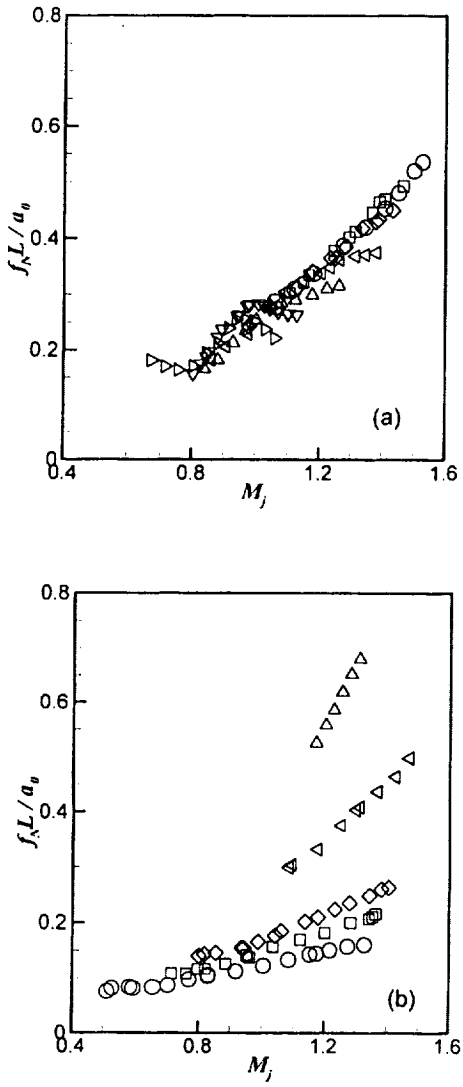

Fig 10 Frequency data of Figs. 9 and 7 plotted in non-dimensional form: (a) data of Fig. 9, (b) data of Fig. 7.

Subsequently, it became apparent that the observed deviation is due to a dependence on the half-angle θ. In Fig. 10(b) there is a progressive deviation of the curves with increasing L that corresponds to a decreasing θ. Note that the data of Fig. 8 would appear the same when plotted as $f_N L/a_0$ versus M_j, since L and a_0 are constants. Those data also indicate a similar trend. With decreasing θ, the slopes of the nondimensional curves become steeper.

The θ-dependence is further addressed in the following. First, the staging behavior is examined here. Four examples of the tone frequency variation over full range are shown in Figs. 11(a) – (d). In each figure, the dimensional frequency data are shown on the top. There are three stages in Fig. 11(a), two each in Figs. 11(b) and (d), and only one in Fig. 11(c). Note that between cases (b) and (d) there is an order of magnitude difference in the nozzle dimensions, commensurate with an order of magnitude difference in the frequencies. Inspection of these as well as other sets of data makes it apparent that stage 1 may be considered as the fundamental in the resonance, stages 2 and 3 being the next odd harmonics. That is, with decreasing M_j, on the left end of stage 1, there is an increase in the frequency by approximately a factor of 3 to begin stage 2. Similarly, on the left end of stage 2, the onset of stage 3 involves a jump by a factor of about 5/3. This becomes clear from the nondimensional data shown at the bottom of each figure (ordinate on right), with appropriate 'correction' for stages 2 and 3. That is, frequencies in stages 2 and 3 have been divided by factors of 3 and 5, respectively. This way, the data for all stages approximately collapsed into one curve. There is a perceptible discontinuity between stages 1 and 2, however, stages 2 and 3 in (a) blended quite well.

That the higher stages are odd harmonics of the fundamental follows duct acoustic resonance characteristics (no flow). For the divergent section (approximately a conical duct 'driven' from the smaller end and open at the other), a fundamental acoustic resonance would correspond to a standing one-quarter wave, with the higher 'stages' occurring at only the odd harmonics. The resonant frequencies can be calculated as (Ref. 23):

$$f_m = \frac{a_0}{4l_p}\sqrt{m^2 + \frac{8l_p}{\pi^2 x_0}}, \quad m = 1,3,5.... \qquad (1)$$

Where, a_0 is the speed of sound,

$$l_p = L + \frac{4D_e}{3\pi}, \text{ and } x_0 = \frac{D_t}{2\tan\theta}.$$

The fundamental and the next harmonic (in kHz) for the four cases of figure 11 turn out to be: (a) 7.8 and 19.6, (b) 0.70 and 1.81, (c) 3.91 and 11.42, and (d) 2.28 and 6.13. While the fundamental lies within the frequency range of stage 1 in (b) and (c), it is much higher than the frequencies of any stage in (a) and lower than the observed frequencies in (d). Note also that the acoustic resonance frequencies are constants whereas here the

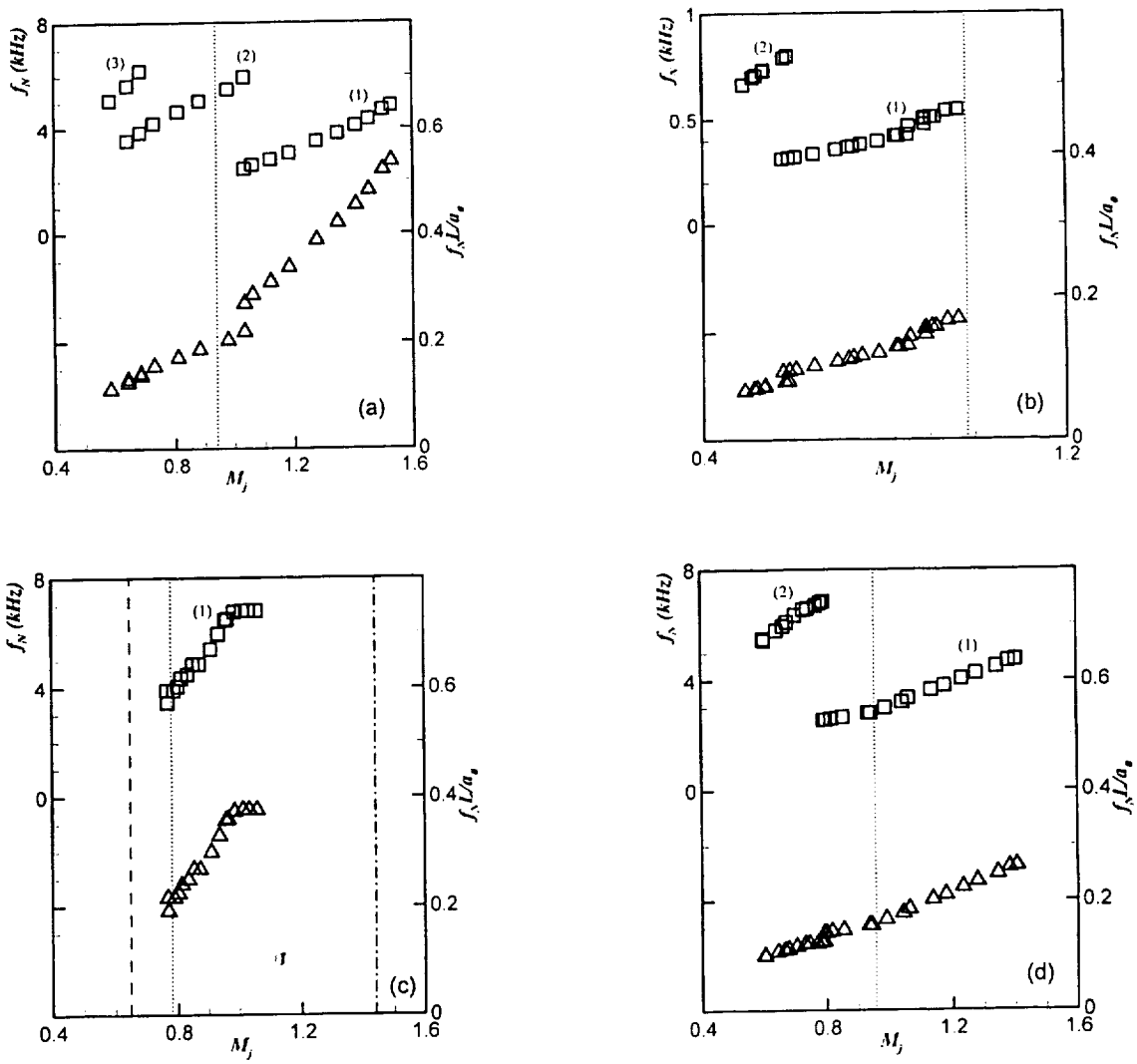

Fig 11 Frequency variation (full range) for four different nozzles. Dimensional data (□) are at the top, corresponding nondimensional data (Δ) with 'stage correction' are at the bottom; numbers in parentheses are stages. (a) Nozzle 2T2, (b) nozzle 5T1, (c) nozzle 6T2, (d) nozzle 1T1.

frequency varies within a stage. Thus, the tones under consideration are not simply due to resonance of the divergent section excited by the flow. The flow field, that is very complex, comes into play. However, the occurrence of only the odd harmonics suggests that the underlying mechanism must be similar to that of acoustic resonance. This is addressed further in the following.

The $f_N L/a_0$ versus M_j curves are constructed from the frequency data for all nozzles, similarly as in Figs 11(a) – (d). A total of seventeen (single, round nozzle) cases, from tables 1 and 2 and the trim cases of Fig. 9, are included in this comparison. The variation in each stage is assumed to be linear. The slopes are estimated by drawing straight lines through the data in each stage. (The data on the ends of a stage departing from linearity are ignored in this process. Also, a few cases with very small θ are excluded since a linear part in the curve is not readily discernible). Simultaneously, the intercepts at $M_j = 1$ are also obtained. As can be seen in Fig. 11, both slope and intercept may vary from stage to stage for a given nozzle. However, there is a consistent dependence on θ. The θ-dependence of the slopes can be seen clearly in Fig. 12. Data for stage 1 are shown by

the triangular symbols while those for stages 2 and 3 are shown by the circular symbols. (The solid data points, identified in the figure caption, will be discussed in §4.2.) In a given stage, the slopes vary inversely as θ. The intercepts also exhibit an inverse functional dependence on θ, as shown in Fig. 13.

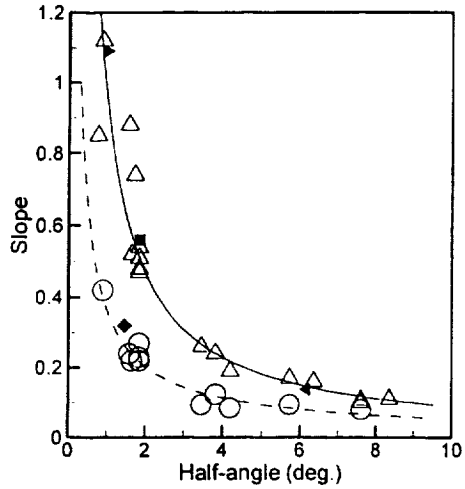

Fig. 12 Slope of $f_N L/a_\theta$ versus M_j for various nozzles, as a function of the half-angle of divergence (θ); Δ, stage 1; O, stages 2 and 3; ■, nozzle 6T1; ◆, nozzle 7T1; ►, Ref. 12; ◄, Ref. 17.

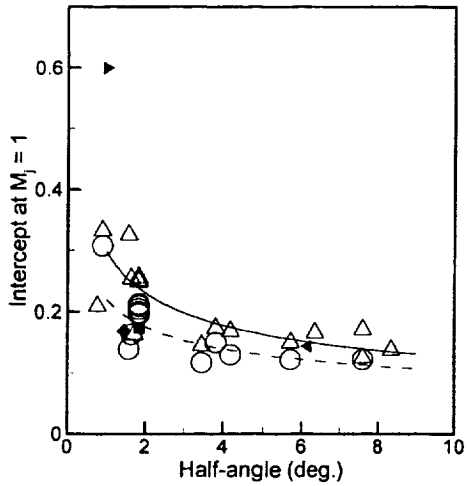

Fig. 13 Intercepts at M_j = 1 corresponding to cases of Fig. 12.

The curves in Figs. 12 and 13 are least-squares-fits through the data for the round nozzle cases (open symbols). From the fitted curves the following equations are obtained, with θ expressed in degrees.

$$\frac{f_N L}{m a_0} = C_1(\theta) + C_2(\theta)(M_j - 1), \qquad m = 1, 3, 5.... \quad (2)$$

$C_1(\theta) = 0.298\ \theta^{-0.370}$, $C_2(\theta) = 0.952\ \theta^{-1.029}$, for stage (1), and

$C_1(\theta) = 0.221\ \theta^{-0.325}$, $C_2(\theta) = 0.363\ \theta^{-0.8375}$, for stage (2).

Frequency for stage 3 (m=5) is also given by the equation for stage (2). Furthermore, the value of M_j where the jump from stage 1 to 2 takes place is also observed to depend on θ. From a similar analysis, the jump location is given by,

$$M_{j\_1\text{-}2} = 1.036\theta^{-0.157}.$$

Note that there are large departures of the data from the average curves especially for the intercept (Fig. 13). Thus, only an estimate of the resonant frequencies may be expected from these correlations. Also, recall that the amplitude of the resonance is relatively ill-defined and sensitive to, e.g., the surface finish of the nozzle's interior. Thus, no attempt is made to correlate the amplitude, however, the frequency seems to be determined mainly by the parameters considered in the foregoing.

3.3 Steady-state characteristics of the internal flow: Applying the temperature-sensitive-paint to the interior surface of the nozzle was a useful tool for exploring the internal flow structure. Unfortunately, the application of this technique for unsteady flow measurement is still under development and only steady-state results could be obtained. They nevertheless provide some insight.

For these experiments, the paint was carefully sprayed on a 'sector' of the interior of the divergent section. The painted strip extended from about the throat to the nozzle exit. The layer of paint was initially about 0.001 in thick. The nonuniformity in the layer was enough to trip the boundary layer for some of the nozzles, resulting in a 'dulling' of the tones. The painted surface had to be polished in order to get the sharp tones back. The picture of the painted strip was taken from outside with a camera angle approximately normal to the nozzle axis. Under filtered blue light (430 nm) the color of the paint responded to the static temperature. Two images were taken – one without flow and another

with flow. A scientific grade CCD camera (512 x 512 pixels) was used to take the images. The data were post-processed by normalizing each pixel level with the corresponding no-flow level. Temperature difference, as small as a fraction of a degree, could be discriminated by the technique.[24]

Figure 14 shows images of the temperature distribution on the painted strip for different values of M_j, for nozzle 3T2. The pictures on the left represent the case of a tripped boundary layer (resonance suppressed). The pictures on the right are the corresponding cases with a smooth interior (resonance on). Bands of color indicating regions of temperature gradients are observed. For the tripped case, a region of strong gradients is observed approximately in the middle of the divergent section. The sharp edge on the right of the dark blue region apparently indicates the location of the shock. In general lower temperatures are expected in regions of high-speed attached flow while higher temperatures are expected in regions of boundary layer separation and in regions past a shock. With resonance,

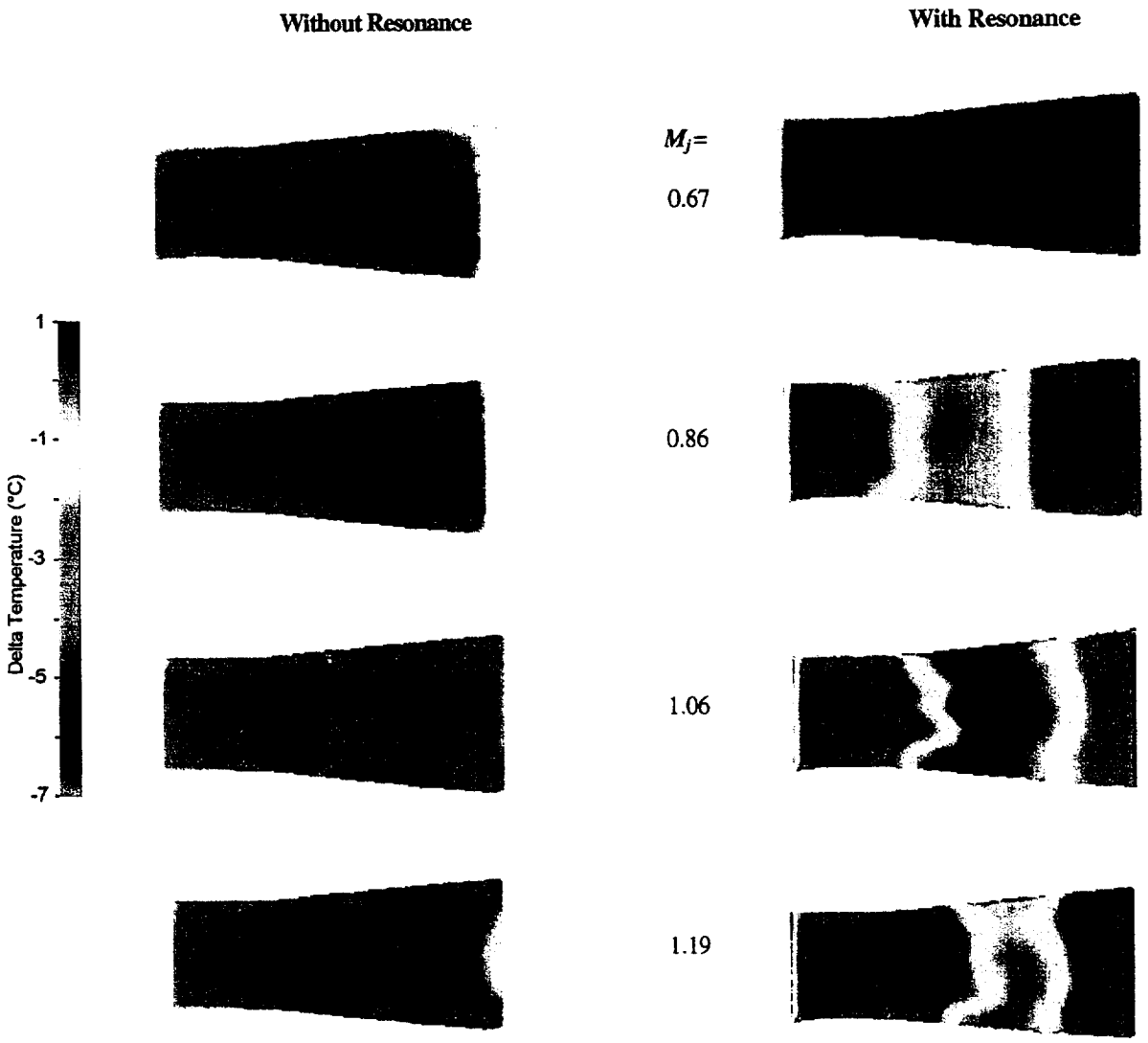

Fig. 14 Interior wall temperature distribution for nozzle 3T2 (D_t = 0.3, D_e = 0.4, L = 0.75), at indicated values of M_j. Left column for tripped boundary layer, right column for smooth interior.

on the right column, the distributions are seen to change significantly. At $M_j = 0.86$, 1.06 and 1.19, a band of warm region (in red and yellow) is observed. This apparently corresponds to a well-defined separation bubble, discussed shortly. Note that the latter three M_j cases represent resonance in stage 1 while at $M_j = 0.67$ resonance in stage 2 takes place (Fig. 3).

The temperature distributions, along an axial line in the middle of the visualized region, are obtained from the data of Fig. 14. These distributions for the tripped and untripped cases are shown in Figs. 15 and 16, respectively. Some of the profiles are annotated for easy later reference. The streamwise distance x is referenced to the nozzle exit, x^* represents the throat location. Let us first examine the trends in Fig. 15.

The temperature is seen to decrease with increasing distance from the throat until at a certain downstream location a relatively abrupt increase takes place. The latter apparently is the location of the 'foot' of the shock intersecting the wall. Upstream of this, the flow is supersonic and the Mach number gradually increases from unity at the throat to some higher value as the shock is approached. The increasing Mach number is accompanied by decreasing static temperature. The static temperature, however, can be calculated to be much lower than the recorded temperatures ('delta temperature' represents static temperature relative to ambient temperature). For example, for a Mach number of 1.2, likely in many of the cases of Fig. 15, the delta temperature would be about -35°C. This contrasts the measured values that are no lower than -7°C. This 'anomaly' is due to the fact that the data represent 'wall temperature' that, in fact, ideally should be equal to the total temperature.

For an adiabatic thermal boundary layer with 'no loss', the wall temperature should be invariant and equal to the total temperature.[25] Why are the measured temperatures low at all? In practice, there are radiation and conduction losses and the wall temperature is always less than the total temperature. For a thermal boundary layer (Crocco-Buseman equation, see cited reference), this is accounted for by a 'recovery factor'. With the assumption of a constant recovery factor, it can be shown that the relative variation in wall temperature is the same as that in core static temperature, albeit the magnitude of the former is only a fraction of the latter.

Since the core static temperature is proportional to the local static pressure, it follows that the measured temperature profiles are similar to corresponding static

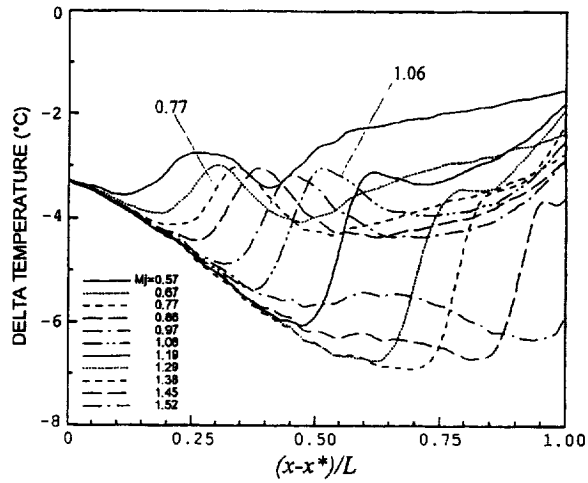

Fig. 15 Axial variation of wall temperature corresponding to the tripped cases of Fig. 14 (resonance suppressed) for indicated values of M_j.

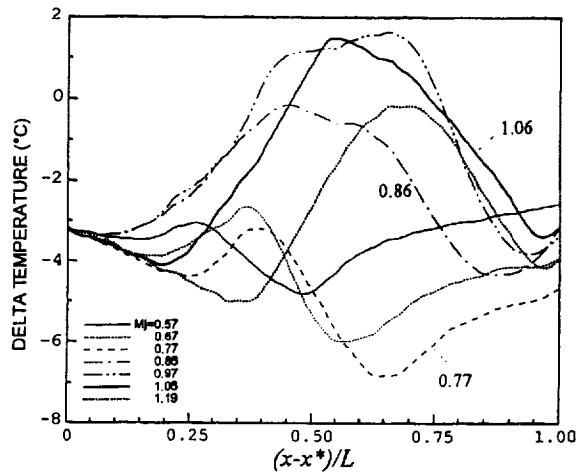

Fig. 16 Axial variation of wall temperature for the cases with smooth interior of Fig. 14 (with resonance).

pressure profiles. In fact, the overall trends in the temperature profiles of Fig. 15 bear striking similarity to static pressure profiles reported in, e.g., Refs. 12, 17, 26. The static pressure also drops with increasing distance from the throat and then rises abruptly past the shock. In the cited references the shock-location was defined by the location of minimum static pressure before the abrupt rise. A similar criterion is applied here to determine the shock location from the temperature minima.

Shock-locations for the tripped case (Fig. 15), obtained by the stated criterion, are plotted in Fig. 17 (circular data points). Note that the abscissa is logarithmic and zero on the ordinate represents the location of the throat. It can be seen that the shock moves down-

stream with increasing M_j, and reaches the exit at $M_j \approx 1.55$. Also shown in Fig. 17 is the theoretical prediction for the shock location based on one-dimensional analysis (solid curve between the dashed and dotted vertical lines). An inspection reveals that, in fact, the shock resides within the nozzle at pressure ratios (or M_j) much higher than that predicted by 1-D analysis. A similar inference is also made from published static pressure data, for example, from Hunter's data for a rectangular C-D nozzle shown in Fig. 18, as well as from the classical 'Stodola experiment' described in Ref. 26 for a circular C-D nozzle.

Referring back to Fig. 16, it can be seen that, with the onset of resonance, the temperature distributions are no longer orderly. The shock location (represented by the temperature minimum) has moved upstream. However, there is a second minimum downstream. For example, at $M_j = 1.06$, the upstream shock has moved from $(x\text{-}x^*)/L = 0.35$ (Fig. 15) to $(x\text{-}x^*)/L = 0.2$ (Fig. 16). (This shift can also be seen in Fig. 17 from the square data points.) Besides the minimum at $(x\text{-}x^*)/L = 0.2$, there is another minimum very near the exit. With the assumption that the latter is the location of boundary layer reattachment, one may infer that a separation bubble exists under the resonant condition. The cases at $M_j = 0.57$, 0.67 and 0.77 involve resonance in stage 2, while the three higher M_j cases involve resonance in stage 1. Stage 1 cases have the downstream minima close to the nozzle exit. In comparison, for stage 2 the second minima occur farther upstream. Thus, a shorter separation bubble is indicated for stage 2 while the bubble length in stage 1 is comparable to L', the distance from the foot of the shock to the exit. (The wall temperature for a few cases in Fig. 16 is somewhat in excess of the ambient temperature. This is thought be due to dissipation within the separation bubble.)

The data presented in this section clarify another aspect of the resonance. Initially, from an examination of the data as in Figs. 1, 3 and 4, it was thought that the resonance might be possible even without a shock inside the divergent section. (The resonance extended well into the 'overexpanded' regime, predicted by one-dimensional analysis). The results discussed here make it amply clear that the flow under consideration is still not overexpanded and that a shock still resides inside the nozzle. In fact, the presence of the shock inside the diverging section turns out to be a necessary condition for the occurrence of the resonance.

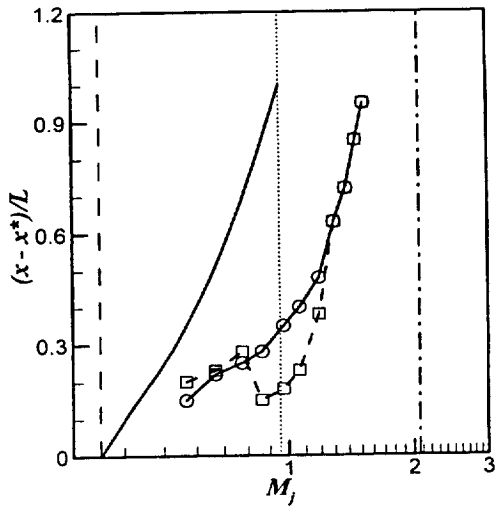

Fig 17 Shock locations versus M_j, inferred from Figs. 15 and 16. O, Tripped case (no resonance); □, smooth interior (with resonance). The solid line on left represents prediction from one-dimensional analysis.

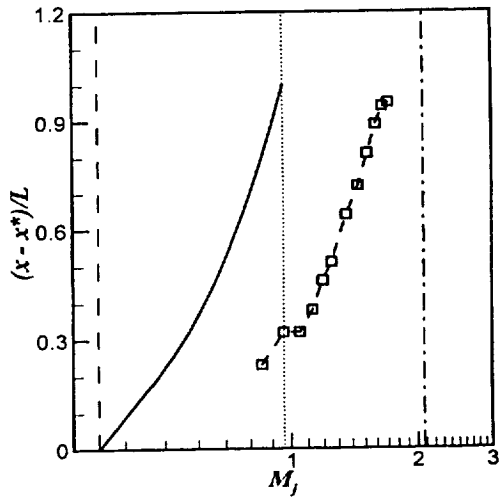

Fig 18 Shock location versus M_j, inferred from wall static pressure data for a rectangular C-D nozzle (Hunter 1999, Ref. 17)

3.4 Unsteady flow characteristics: The unsteady flow characteristics were explored with a miniature pressure transducer for nozzle 5T1. For the purposes of completeness, the coordinates of this nozzle are listed in table 3. The larger nozzle size enabled the measurements without significant probe interference. The transducer was mounted on a 9 in long support that tele-

scoped from a root diameter of 0.25 in to the sensor diameter of 0.063 in. It was inserted straight into the flow (as with a Pitot probe) from a streamlined support mounted on a computer controlled traversing mechanism. The probe essentially responded to the unsteady total pressure. A ¼ in (B&K) microphone, placed just outside the flow and near the lip of the nozzle, provided a reference signal for these measurements. Two flow conditions were chosen for the exploration: (a) M_j = 0.55 yielding a resonant frequency of 755 Hz (stage 2), and (b) M_j = 0.75 yielding a resonant frequency of 385 Hz (stage 1); the frequency variation for this nozzle has been shown in Fig. 11(b).

Table 3 Co-ordinates (inches) for nozzle 5T1

x-x^*	R	x-x^*	R
-6.3527	1.7941	0.9102	1.3651
-5.0632	1.6892	1.1658	1.3955
-3.7736	1.6044	1.4761	1.4348
-2.4840	1.5171	1.7833	1.4752
-1.6243	1.4462	2.1915	1.5285
-0.7646	1.3574	2.6296	1.5841
-0.3347	1.3042	3.0146	1.6300
0.0000	1.2823	3.3656	1.6690
0.3210	1.3046	3.8263	1.7157
0.6134	1.3326	4.1996	1.7500

The centerline (time-averaged) total and static pressure variations, measured with appropriate probes in separate runs, are first shown in Fig. 19. Data are shown for the two operating conditions. The trend in the static pressure data is similar to that discussed before in §3.3. According to the criterion discussed, the shock location is just downstream of the throat at the lower M_j and at about x/L = -0.8 at the higher M_j. The total pressure data exhibit a drop-off near the location where static pressure rises. However, the start of the drop-off is close to each other for the two values of M_j whereas the rise in the static pressure is farther downstream at the higher M_j. The fact that total pressure is a 'point function' while static pressure is approximately the same across a given cross-section might explain some of these trends. Following the drop-off after the shock, the total pressure basically remains constant over the measurement domain. Note that the data are shown from somewhat upstream of the throat to about 0.8L downstream of the nozzle exit.

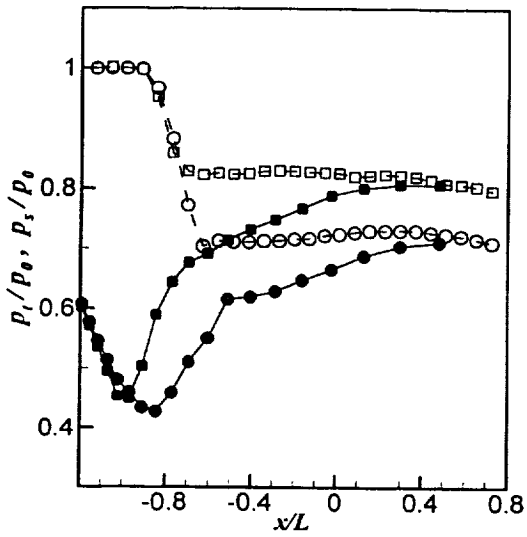

Fig. 19 Centerline variations of total (open symbols) and static pressure (closed symbols) for nozzle 5T1 (D_t = 2.565, D_e = 3.5, L = 4.2): □, M_j = 0.55 (f_N = 755 Hz); O, M_j = 0.75 (f_N = 385 Hz).

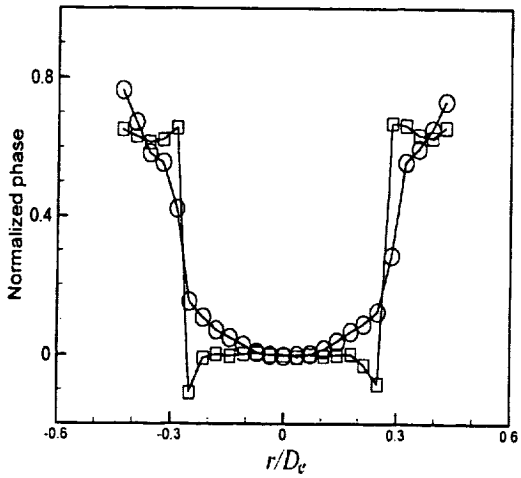

Fig. 20 Radial profiles of phase at x/D_e = 0.25 for nozzle 5T1: □, M_j = 0.55 (f_N = 755 Hz); O, M_j = 0.75 (f_N = 385 Hz).

Diametral profiles of the fundamental phase, (i.e., mode shape at the fundamental frequency), are shown in Fig. 20. The data are for a streamwise location just downstream of the nozzle exit. The phase is measured through spectrum analysis of the transducer signal, relative to the fixed microphone signal. Ignoring some difference in details, it is clear that the resonance at either stage involves axisymmetric unsteady fluctuations.

As reported in Ref. 14, cursory measurements with several other nozzles and operating conditions also indicated axisymmetric shapes. The rectangular case included in Fig. 1 also indicated a symmetric shape.

Phase-averaged amplitude of the unsteady total pressure was measured at various axial locations. The measurements were carried out on the axis at 27 equally spaced locations covering the same range as in Fig. 19. At each location, 39 phase-averaged data were recorded approximately over $1.2T$, T being the period corresponding to the resonant frequency. Sample data for the flow inside the nozzle are shown in Figs. 21(a) and (b) for $M_j = 0.55$ and 0.75, respectively. The ordinates are in approximate percentage of the plenum pressure. (Some measurement difficulty, not critical in the present context, has been discussed in Ref. 14). One finds that quite large fluctuations take place – as much as ±20 percent in stage 1 at $M_j = 0.75$ in (b).

Note that the data in Fig. 21 cover an axial range from x/L = -0.6 to about the nozzle exit. Farther upstream, the amplitudes drop rapidly. There, the small amplitudes are somewhat contaminated by probe interference especially when the probe is near the shock (as evident from some variation in the reference signal). Thus, those data are not shown in full detail and only the overall (r.m.s.) amplitudes are discussed in the following. Downstream of the nozzle, within the measurement domain, the waveform basically remains the same as seen at the nozzle exit. There is some amplification accompanied by systematic change in phase with increasing x. Those data are also not shown since they are not central to the present discussion.

In each of Figs. 21(a) and (b), the waveforms are complex. For the resonance in stage 1 (Fig. 21b), there is very little phase shift within the measurement range (covering $0.65L$). The phase shift for stage 2 (Fig. 21a), up to about x/L = -0.31, is also small; however, farther downstream there is a systematic phase shift with increasing x. Note that the waveforms are far from sinusoids and there is large harmonic distortion. The processes leading to the complex waveforms remain ill-understood. However, the negligible phase shift indicates that these are standing waves within the nozzle. If the data in Fig. 21(b), for example, represented traveling waves and the x-range covered corresponded to ¼ wavelength, the curves marked "1" and "0" would be separated by approximately 90 degrees ($t/T = 0.25$).

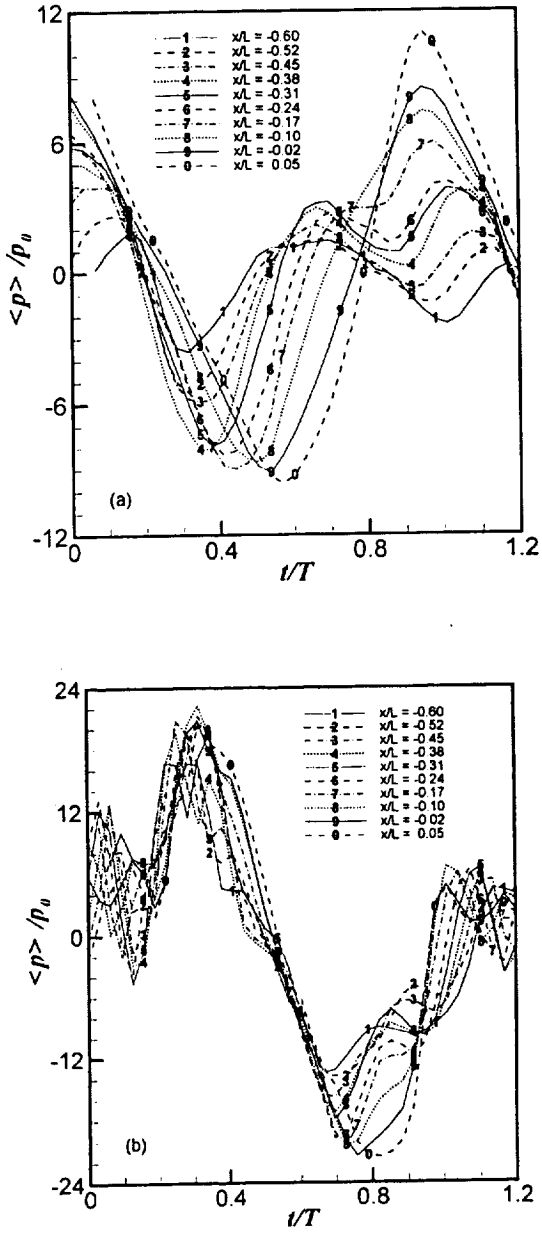

Fig. 21 Phase-averaged total pressure variations with time at indicated x-locations; time is normalized by the period (T) and ordinate is approximately in percent of plenum pressure (p_0). Data are for nozzle 5T1: (a) $M_j = 0.55$ (f_N = 755 Hz); (b) $M_j = 0.75$ (f_N = 385 Hz).

This clearly is not the case. The notion that the resonance involves standing waves is further supported by the overall amplitude variations shown in Fig. 22.

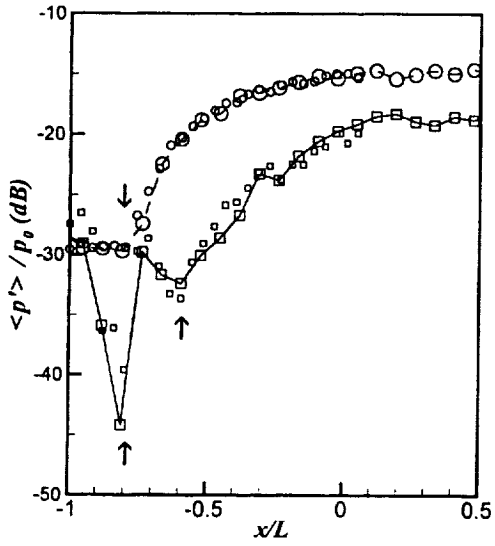

Fig. 22 Centerline variations of phase-averaged r.m.s. amplitude at the fundamental frequency, nozzle 5T1: □, M_j = 0.55 (f_N = 755 Hz); ○, M_j = 0.75 (f_N = 385 Hz).

For acoustic resonance of the diverging section (§3.2) the fundamental should correspond to a standing one-quarter wave. This would involve a pressure node at the exit and an antinode near the throat. The next 'stage', the third harmonic, should also have a node at the exit and an antinode at the throat; however, there should be an additional node in between. The nodes and antinodes for velocity fluctuation would be the reverse, i.e., a pressure node would correspond to velocity antinode and vice versa. Such a nodal pattern is also indicated in the present flow. The (r.m.s.) amplitude, computed by integration of the phase-averaged data over the period (T), is shown in Fig. 22, for the two operating conditions. Even though the amplitudes at the upstream locations are small (note the logarithmic scale), and thus prone to contamination by the slightest probe interference, two nodes are apparent for stage 2 (square data points). These are identified in the figure by the upward pointing arrows. On the other hand, stage 1 (circular data points) involves only one node around x/L = -0.8, identified by the downward pointing arrow. (The smaller symbols in this figure represent a repeat of the experiment with finer resolution). The data of Fig. 22 lend further credence to the notion that stages 1 and 2 involve standing one-quarter and three-quarter wave patterns, commensurate with the observed staging behavior in the frequency variation.

4. Discussion and summary

4.1 Comparison of results from past experiments

Reference 12: As mentioned in the introduction, a series of experiments was conducted about twenty years ago for transonic flow through a diffuser by M. Sajben and coworkers (Refs. 10-12). They studied a 'low-frequency, self-excited oscillation' occurring in the diffuser. The phenomenon appears very similar, if not the same, as the one addressed here. Thus, those results merit a special review. Their flow geometry involved 'one-half' of a two-dimensional diffuser. That is, the floor was flat, the upper wall was convergent-divergent and the two sidewalls were parallel. In successive experiments the dimensions were varied; the results of Ref. 12 are most pertinent. The throat height (H) was 1.73 in and the15 in long diverging section ended with a height of 2.64 in. Following the diverging section there was a parallel section (constant height) of 10 in length. Experiments were also conducted by extending the length of the parallel section another 28 in. At the exit of the apparatus the flow discharged into the ambient, similarly as in the present experiment. Detailed measurements were conducted, e.g., on the unsteady wall pressure characteristics with accompanying flow visualization of the unsteady shock.

They observed multiple spectral peaks in the pressure fluctuations at low supply pressures but a single, strong peak at higher supply pressures. Through cross correlation measurements and analysis they inferred that the multiple peaks at low supply pressures were longitudinal duct resonance (fundamental and odd harmonics). However, the frequency of the peak at the higher pressure remained invariant for both duct lengths (L/H = 14.4 and 30.5), and thus, they inferred that it 'did not follow acoustic predictions.' However, the frequency variation shown for the smaller length (their figure 10) does show an increasing frequency with increasing operating pressure within an M_j range of 0.5 to 0.7 (values of M_j inferred from cross reference to their figure 3). These data apparently correspond to stage 1 oscillation and are discussed further in §4.2. The observation that the fundamental and the odd harmonics prevail at the lower pressure is also in accordance with the present results.

It is not clear why the additional length after the diverging section did not affect the frequency in stage 1. It is possible that the boundary layer bleed just downstream of the diverging section, employed in their ex-

periment, imposed a length-scale that remained unchanged regardless of the geometry downstream. Another significant difference is the fact that they had a boundary layer trip at the inlet section; the resonance took place in spite of the trip. Again, there was a boundary layer bleed following the trip. Furthermore, the trip was located quite far upstream (x/H = -6.93), possibly explaining why the resonance took place regardless.

Reference 17: In this work, steady state results were presented for the characteristics of the internal flow of a convergent-divergent, rectangular nozzle (see also Ref. 27). The nozzle had a throat area of 4.317 in^2, an expansion ratio of 1.797 and a constant width of 3.99 in. While analyzing the internal shock structure, the author noted a flow unsteadiness at relatively lower operating pressures. Fortunately, during Schlieren flow-visualization experiment an audio signal from a microphone was recorded simultaneously with the video records. The author kindly provided these records. An analysis of the audio signal revealed spectral peaks very similar to those observed in the present study. This is shown in Fig. 23. The single peak at $M_j = 0.71$ is apparently due to stage 1 resonance. The frequency increases with increasing M_j and a small peak is detectable at $M_j = 0.96$. At the lowest M_j, spectral peaks apparently for both stages 1 and 2 are present.

The Schlieren video records provided by C. A. Hunter, as well as those shown in Ref. 12, allow an insight into the unsteady shock motion associated with the resonance. Sample video records for the case of M_j = 0.71 (Fig. 23) are shown in Fig. 24. The flow is from left to right, and the shock can be seen downstream of the throat. The two pictures approximately capture the extrema in the shock locations during its unsteady motion. The shock is complex with a 'lambda foot' and changes in shape quite drastically within the oscillation cycle. Corresponding video records at $M_j < 0.57$ (stage 2) indicated a single shock closer to the throat. However, at $M_j = 0.57$, the shock structure was complex and involved multiple shocks, presumably commensurate with the multiple peaks in the spectra. On the other hand, at $M_j = 0.96$, a 'cleaner' shock with a well defined 'lambda foot' occurred farther downstream. These data provide a basis of discussion in §4.2.

Reference 16: Another past work, that of Meier, also merits a comment. An unsteady flow oscillation in a

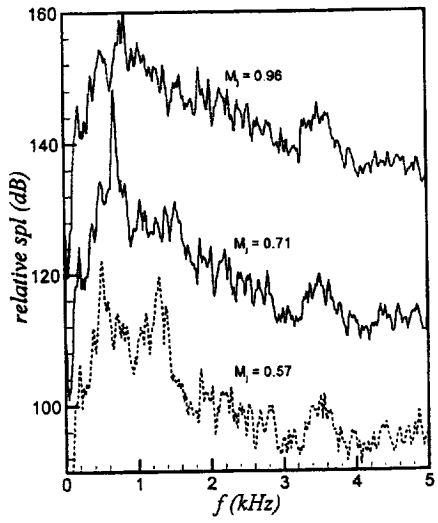

Fig. 23 Sound pressure spectra from the experiment of Ref. 17.

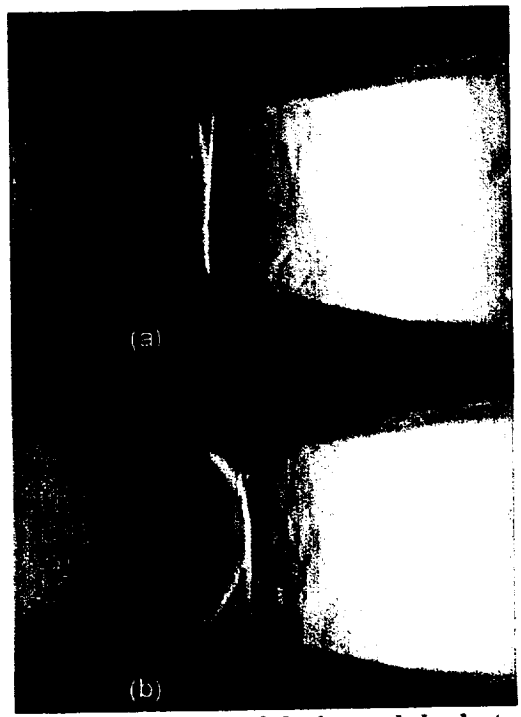

Fig. 24 Schlieren pictures of the internal shock structure for the M_j = 0.71 case of Fig. 23 (Ref. 17); (a) and (b) for two arbitrary times.

two-dimensional C-D nozzle was reported in this work. Vivid flow visualization pictures, showing the shock motion and boundary layer separation, over a cycle of the oscillation were presented. A scrutiny reveals that

the boundary layer separation tended to occur on one wall. This contrasts the 'symmetric' oscillations noted in the present experiment (§3.4). It is not clear if the observed unsteady flow was similar to the resonance studied here. If it is, it may suggest that nonsymmetrical modes are also possible especially with the rectangular geometry.

4.2: Frequency scaling for rectangular and co-annular nozzles: Data from three rectangular nozzles have been discussed so far: nozzle 6T1 and those of Refs. 12 and 17. In all three cases the divergence was in one lateral direction while the walls in the other direction were parallel. The frequency characteristics of these as well as the co-annular nozzle (7T1) are discussed now in comparison to the correlations in Figs. 12 and 13,. For the comparison, an equivalent half-angle of divergence, θ_{eq}, is defined as follows. With H_t and H_e denoting the heights at the throat and exit, respectively, equivalent diameters D_t and D_e are first determined from the areas $(H_t + H_e)*H_t/2$ and $(H_t + H_e)*H_e/2$. The value of θ_{eq} is then obtained similarly as in the circular case ($=\tan^{-1}(D_e - D_t)/2L$). With θ_{eq} defined this way, the rate of flow divergence with increasing streamwise distance becomes comparable to that for a circular case where the flow diverges circumferentially.

For the data of Fig. 23, the average slope of fL/a_0 versus M_j was calculated from the spectral peaks at $M_j = 0.57$ (488 Hz) and $M_j = 0.96$ (825 Hz). The intercept at $M_j = 1$ was obtained by extrapolation. The same procedure was followed to approximately obtain these values from Ref 12 (utilizing their figures 10 and 3). These results, as well as that for the co-annular case, have been shown in figures 12 and 13 by the solid symbols. The index m=1 (Eq. 2), used in plotting these data, yielded the best match with the correlation equations. This, together with an inspection of the raw frequency data (no further sign of frequency jump with increasing M_j), quite clearly indicated that the data under consideration for all four cases belonged to stage 1.

It is apparent that the slope and intercepts for the rectangular cases are well represented by the correlation equations. Data for the co-annular case exhibit some deviation. It is possible that the inner flow in the latter case exerts some influence on the pressure gradients and the shock structure within the outer annulus. Nevertheless, the agreement with the average data trend is quite well for all four cases. Thus, Eq. (2) should be useful for predicting the resonant frequencies useful for predicting the resonant frequencies for a variety of nozzle geometry.

4.3 Possible mechanism: A full understanding of the mechanism of the phenomenon and, hence, an analytical formulation for prediction of its characteristics have remained illusive. However, from the accumulated evidence the following may be said:

The phenomenon requires a shock to be present in the diverging section. Following the shock there are boundary layer separation and a separation bubble. Probable flow fields are sketched in Fig. 25 for the two conditions of Figs. 19-22. Results of Figs.15 and 16, together with observations of Refs. 12 and 17, aided in constructing these flow fields. A smaller separation bubble is likely at the lower M_j as suggested by the wall temperature data of Fig. 16. At the higher M_j, with the onset of stage 1, it is possible that the shock has developed a 'lambda foot' that would explain the upstream shift of the 'shock location' seen in Figs. 16 and 17. Such shock structures and separation bubble characteristics were also reported in Ref. 12.

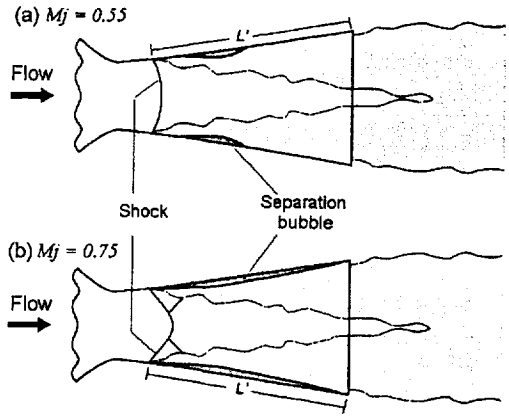

Fig. 25 Schematic of likely flow fields (a) M_j = 0.55, f_N = 755 Hz (stage 2); (b) M_j = 0.75, f_N = 385 Hz (stage 1).

The unsteadiness of the shock, owing to the unsteadiness of the bubble, serves as a source of perturbation. Two possibilities may be considered. (1) The separated boundary layer in the subsonic region downstream of the shock supports instability wave growth. The downstream propagating instability (vorticity) wave, upon interaction with the discontinuity at the nozzle exit, sends a feedback wave. This feedback wave travels at acoustic speed through the separated boundary layer.

This, upon reaching the foot of the shock, completes the feedback loop. In Ref. 14, this was conjectured to be the mechanism. (2) The mechanism is similar to that involved in longitudinal acoustic resonance. The shock becomes the 'source' of perturbation (like a diaphragm driving the flow). Resonance occurs at a frequency when the right impedance condition (least 'resistance') is satisfied.[23] An antinode in pressure fluctuation occurs just downstream of the shock while a node occurs near the nozzle exit. The fundamental corresponds to the case when one-quarter wavelength is fitted within the distance from the foot of the shock to the nozzle exit (L').

It is apparent that accumulated evidence points to (2) as the likely mechanism. The main difficulty with (1) is that it stipulates one full wavelength be contained within the length L' at the fundamental, resonance being possible at all higher harmonics. The results presented in the foregoing indicate that the fundamental in fact corresponds to a one-quarter-wave resonance, commensurate with (2). Furthermore, even harmonics are absent and resonance at only the odd harmonics takes place.

Certain trends in the data can now be explained qualitatively. Consider a low supply pressure when there is a resonance in stage 2. The shock is somewhere downstream of the throat and a separation bubble exists farther downstream (Fig. 25a). A standing '¾ - wave' is involved. The distance from the foot of the shock to the exit of the nozzle (L') imposes the length-scale while a combination of the phase speeds of the downstream and upstream propagating waves imposes the time-scale. Much of the observations can be reconciled simply by considering the variation of L'. As the supply pressure is increased, the shock moves downstream resulting in a decrease in L'. This is followed by a decrease in the wavelength and hence an increase in the frequency. With further increase in supply pressure, the length L' can no longer support ¾-waves. In order to satisfy appropriate impedance conditions (stipulating the node / antinode locations), the resonance drops to the fundamental. This is accompanied by a decrease in the frequency by approximately a factor of 3. With further increase in the supply pressure, there is again a decrease in L' resulting in an increase in the frequency. The resonance ceases when the shock-induced separation location has moved sufficiently downstream so that the flow field can no longer support the '¼-wave'.

A qualitative explanation can also be given with similar reasoning for the observed θ-dependence of the frequency variation curves. Consider that the flow is just choked at the throat at a certain supply pressure. In order to move the shock from the throat to the exit a finite differential pressure is required for a given geometry of the divergent section. The required differential pressure to achieve this should be smaller for smaller value of θ. This can be appreciated by considering the limiting case of $\theta = 0$, when an infinitesimal differential pressure should move the shock from the throat to the exit. Thus, with increasing supply pressure, the rate of decrease in L' is faster when θ is smaller. This would translate into a steeper slope of the frequency variation with M_j, for smaller θ.

Finally, it is possible that on a first approximation Eq. (1) given in §3.2 might be applicable for prediction of the frequency, after having the length-scale L replaced by L'. The characteristic dependence of L' on M_j and θ, as discussed in the foregoing, would qualitatively explain the observed frequency variations. The functional dependence of L'/L on M_j and θ, obtained with some simplification and combination of Eqs. (1) and (2), could be checked against the experimental data. However, much remains unknown, such as the dependence of the phase speeds on the flow parameters. While Eq. (1) is for no-flow condition an analytical solution with even a simple uniform flow is intractable, to the authors' knowledge. Here, the flow is much more complex. Thus, further efforts to arrive at a rational set of equations for the prediction of the frequency was not considered at this time.

4.4 Summary: The subject phenomenon takes place when there is a shock in the diverging section of the nozzle. The distance from the foot of the shock to the exit of the nozzle imposes the length-scale, L'. The frequency variation exhibits a staging behavior. The fundamental (stage 1) occurs at relatively large supply pressures and corresponds to a standing one-quarter wave. With decreasing pressure, higher stages at only the odd harmonics take place. For all stages, the unsteady fluctuations are found to be of the axisymmetric shape in this experiment.

The frequency characteristics are found to depend on the half-angle of divergence of the nozzle, θ. With smaller angle the slope of the frequency variation

with M_j becomes steeper. The trends in the frequency variation are qualitatively explained simply from the characteristic variation of the length-scale L'. In a given stage, the shock moves downstream with increasing supply pressure; thus, a decreasing L' leads to an increasing frequency. When θ is smaller, the shock is pushed downstream at a faster rate with increasing supply pressure; the faster decrease in L' explains the steeper slope of the frequency variation curve.

From a collection of data, correlation equations are provided for the prediction of the frequency for single round nozzles. These equations also satisfactorily predict the resonant frequencies for non-axisymmetric nozzles when the angle-of-divergence is determined properly.

The resonance depends on the characteristics of the boundary layer prior to the shock-induced separation. Boundary layer tripping at locations upstream of the separation tends to suppress the resonance. It is likely that this effect occurs through a disruption of the azimuthal coherence of the perturbation. The trip effect provides an engineering solution for avoiding the resonance as well as reducing 'internal noise' arising from an intermittent occurrence of the resonance. There is a potential for noise benefit simply by suitable tripping of the boundary layer just prior to and aft of the nozzle's throat.

Acknowledgement

Aerospace Propulsion and Power Research and Technology Base program, under Task Y0M1367, have supported this work.

References

1. Hill, W.G. and Greene P.R., "Increased turbulent mixing rates obtained by self-excited acoustic oscillations", *Trans. ASME, J. Fluids Engr.*, **99**, p.520, 1977.
2. Hussain, A.K.M.F. and Hasan, M.A.Z., "The 'whistler-nozzle' phenomenon", *J. Fluid Mech.*, **134**, p.431, 1983.
3.Witczak, K.J., "Self-excited oscillations of gas flow in a duct", Nonlinear vibration problems, No. 18, pp. 147-207 (Politechnika, Warsaw, Poland), A78-17768, 1977.
4. Krothapalli, A. and Hsia, Y.C., "Discrete tones generated by a supersonic jet ejector," *J. Acoust. Soc. Am.*, 99(2), p.777, 1996.
5. Powell, A., "On the mechanism of choked jet noise," *Proc. Phys. Soc. London*, 66, pp. 1039-1056, 1953.
6. Tam, C.K.W., "Supersonic jet noise," *Ann. Rev. Fluid Mech.*, 27, pp. 17-43, 1995.
7. Raman, G., "Advances in understanding supersonic jet screech: review and perspective," *Progress in aerospace Sciences (Including Aircraft Design)*, vol. 34, pp. 45-106, 1998, (also, *AIAA Paper* No. 98-0279, 36th Aerospace sciences Meeting, Reno, NV, Jan. 12-15, 1998)
8. J.M. Seiner, NASA Langley Research Center, 1998, private communication.
9. Zaman, K.B.M.Q. and Dahl, M.D., "Some observations on transitory stall in conical diffusers," *AIAA paper 90-0048*, 28th AIAA Aerospace Sciences meeting, 1990.
10. Chen, C.P., Sajben, M., Kroutil, J.C., "Shock-wave oscillations in a transonic diffuser flow," *AIAA J.*, 17 (10), pp. 1076-1083, 1979.
11. Sajben, M., Bogar, T.J. and Kroutil, J.C., "Unsteady transonic flow in a two-dimensional diffuser," *AFOSR Report* TR-80-0628, May 1980.
12. Bogar, T.J., Sajben, M. and Kroutil, J.C., "Characteristic frequencies of transonic diffuser flow oscillations," *AIAA J.*, 21 (9), pp. 1232-1240, 1983.
13. Hsieh, T. and Coakley, T.J., "Downstream boundary effects on frequency of self-excited oscillations in transonic diffuser flows," *AIAA Paper* no. 87-0161, 25th Aerospace Sciences Meeting, Reno, NV, Jan. 12-15, 1987.
14. K.B.M.Q. Zaman and M.D. Dahl, "Aeroacoustic resonance with convergent-divergent nozzles," *AIAA Paper* 99-0164, 37th AIAA Aerospace Sciences Meeting, Reno, NV, January 11-14, 1999.
15. K.B.M.Q. Zaman and D. Papamoschou, "Study of mixing enhancement observed with a co-annular nozzle configuration," *AIAA Paper* 2000-0094, 38th AIAA Aerospace Sciences Meeting, , Reno, NV, January 10-13, 2000.
16. Meier, G.E.A., "Shock induced flow oscillations," *AGARD Proc. Flow Separation*, No.168, 1974.
17. Hunter, C.A., "Experimental, theoretical, and computational investigation of separated nozzle flows," *AIAA Paper* No., 98-3107, 34th Joint Propulsion Conf., Cleveland, OH, July 13-15, 1998.
18. Nakamura, Y., "Some contributions on a control-surface buzz at high subsonic speeds," *J. Aircraft*, 5(2), 1968.
19. Mabey, D.G., "Some remarks on buffeting," Royal Aircraft Establishment, RAE TM Structures 980, February 1981. (Also, "Unsteady airloads and aeroelastic problems in separated and transonic flows," *AGARD* Conference, Brussels, March 1981).
20. Culick, F.E.C., "Oscillatory and unsteady processes in liquid rocket engines," *Proc. Combustion Instability in Liquid Rocket Engines* (ed. H. F. R. Schoyer), European Space Agency Rep. WPP-062, 1993.
21. Zaman K.B.M.Q., "Spreading characteristics and thrust of jets from asymmetric nozzles," *J. Fluid Mech.* 1999.
22. Samimy, M., Zaman, K.B.M.Q. and Reeder, M.F., "Effect of tabs at the nozzle lip on the flow and noise field of an axisymmetric jet," *AIAA J., 31*(4), pp. 609-619, 1993.

23. Morse, P. M., "Vibration and Sound," *McGraw Hill*, NY, 1948.
24. Liu, T., Campbell, B., Burns, S., and Sullivan, "Temperature- and Pressure-sensitive luminescent paints in aerodynamics," *Applied Mechanics Reviews*, Vol. 50, No. 4, 227-246, 1997.
25. Schlichting, H., "Boundary-layer theory," *McGraw Hill*, NY, 7th Edition, 1979.
26. Anderson, J. D., "Modern compressible flow with historical perspective," *McGraw Hill*, NY, 1982.
27. Hunter, C.A, "An Experimental Analysis of Passive Shock - Boundary Layer Interaction Control for Improving the Off-Design Performance of Jet Exhaust Nozzles," M.S. Thesis, The George Washington University / NASA Langley Research Center, September 1993.